

Quantification of benzo[*a*]pyrene diol epoxide DNA-adducts by stable isotope dilution liquid chromatography/tandem mass spectrometry

Qian Ruan¹, Hye-Young H. Kim¹, Hao Jiang¹, Trevor M. Penning¹, Ronald G. Harvey² and Ian A. Blair^{1*}

¹Center for Cancer Pharmacology, University of Pennsylvania School of Medicine, 854 BRB II/III, 421 Curie Boulevard, Philadelphia, PA 19104-6160, USA

²The Ben May Institute for Cancer Research, The University of Chicago, Chicago, IL 60637, USA

Received 26 January 2006; Revised 27 February 2006; Accepted 27 February 2006

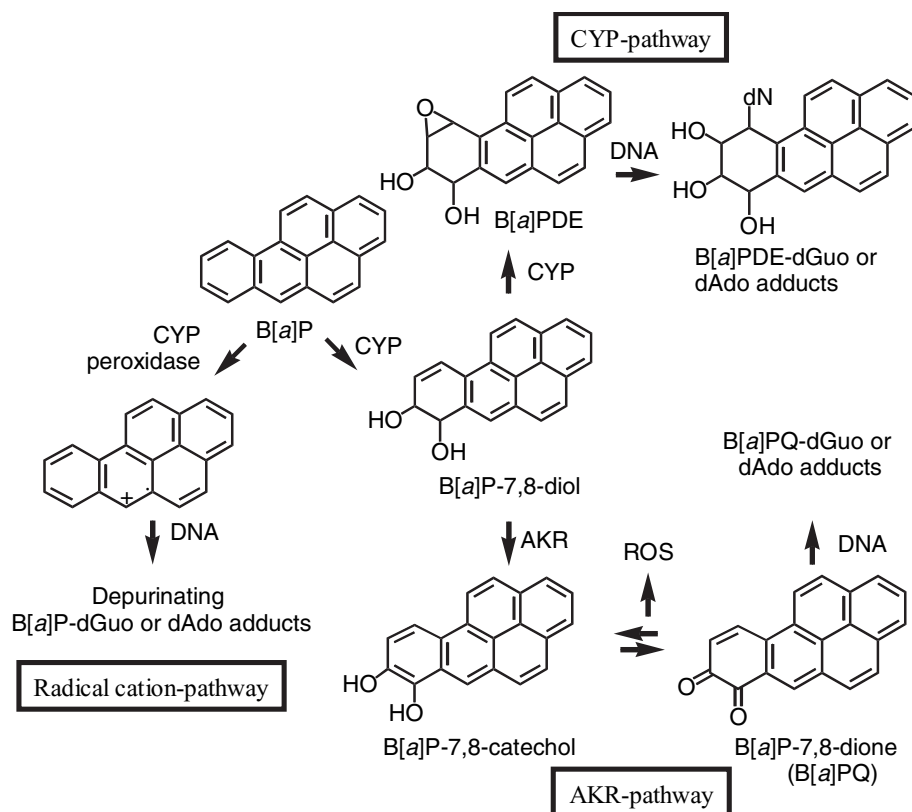
Polycyclic aromatic hydrocarbons (PAHs) are ubiquitous environmental pollutants found in car exhausts, charbroiled food, and tobacco smoke. Three pathways for the metabolic activation of B[*a*]P to ultimate carcinogens have been proposed. The most widely accepted pathway involves cytochrome-P450 (CYP) 1A1- and/or 1B1-mediated formation of B[*a*]P-7,8-oxide, which undergoes epoxide hydrolase-mediated metabolism to the proximate carcinogen B[*a*]P-7,8-dihydro-7,8-diol. Further CYP1A1- and/or CYP1B1-mediated activation of the dihydrodiol results in the formation of 7,8-dihydroxy-9,10-epoxy-7,8,9,10-tetrahydrobenzo[*a*]pyrene (B[*a*]PDE), the ultimate carcinogen. In previous studies, it was demonstrated that (+)-*anti*-B[*a*]PDE was the most potent tumorigen of the CYP-derived B[*a*]PDE diastereomers. We have developed a stable isotope dilution, liquid chromatography multiple reaction monitoring/mass spectrometry (LC-MRM/MS) assay for all eight (±)-*anti*-B[*a*]PDE-derived dGuo and dAdo DNA-adducts. The LC-MRM/MS assay was rigorously validated and used to show that (+)-*anti-trans*-B[*a*]PDE-dGuo was the major adduct formed when naked DNA and human bronchoalveolar adenocarcinoma H358 cells were treated with (±)-*anti*-B[*a*]PDE. The preference for DNA-adducts derived from (+)-*anti*-B[*a*]PDE was even more apparent in cellular DNA. Thus, the increased potency of (+)-*anti*-B[*a*]PDE as a tumorigen is most likely due its ability to preferentially form DNA-adducts when compared with (–)-*anti*-B[*a*]PDE. Also, the adduct profile suggests that this occurs by binding of (+)-*anti*-B[*a*]PDE to DNA in a manner that facilitates covalent binding to dGuo rather than dAdo residues. Copyright © 2006 John Wiley & Sons, Ltd.

Polycyclic aromatic hydrocarbons (PAHs) are a family of planar aromatic compounds that are formed by a variety of combustion processes.¹ These ubiquitous environmental pollutants are found in car exhausts, charbroiled food, and tobacco smoke.^{2–4} High occupational exposure to PAHs occurs in workers involved in aluminum production, iron and steel foundries, fossil fuel processing, wood impregnation, roofing, and road paving.⁵ Substantial evidence has accrued to show that PAHs are causative agents in lung,^{6,7} skin,^{8,9} and bladder cancer.^{8,9} PAHs are not carcinogenic in their own right but require metabolic activation.¹⁰ Three pathways for the activation of PAHs to their ultimate carcinogens have been proposed.^{10–14} These pathways are shown in Scheme 1 for benzo[*a*]pyrene (B[*a*]P), a major PAH found in tobacco smoke.¹ The most widely accepted pathway of activation involves cytochrome-P450 (CYP)-mediated formation of B[*a*]P-7,8-oxide,

which undergoes epoxide hydrolase mediated hydrolysis to the proximate carcinogen B[*a*]P-7,8-dihydro-7,8-diol (B[*a*]P-7,8-dihydrodiol).^{10,11} CYP1A1 and CYP1B1 are considered to be the major CYPs involved in the activation of B[*a*]P,^{15,16} although other isoforms including CYP1A2 are able to metabolize B[*a*]P.^{16,17}

Further activation of B[*a*]P-7,8-dihydrodiol can occur through CYP1A1- or CYP1B1-mediated metabolism to form the ultimate carcinogen, 7,8-dihydroxy-9,10-epoxy-7,8,9, 10-tetrahydrobenzo[*a*]pyrene (B[*a*]PDE).^{17,18} It has also been demonstrated that B[*a*]PDE can arise through co-oxygenation of B[*a*]P-7,8-dihydrodiol during prostaglandin biosynthesis,¹⁹ or through lipid peroxy-radical mediated epoxidation.²⁰ The B[*a*]PDE is detoxified by hydrolysis to the corresponding tetrols^{1,13,21} or by glutathione-S-transferase-mediated conversion into GSH-adducts.^{1,22} Any B[*a*]PDE

*Correspondence to: I. A. Blair, Center for Cancer Pharmacology, University of Pennsylvania School of Medicine, 854 BRB II/III, 421 Curie Boulevard, Philadelphia, PA 19104-6160, USA.
E-mail: ian@spirit.gcrc.upenn.edu
Contract/grant sponsor: NIH; contract/grant number: P01 CA 92537.



Scheme 1. Metabolic pathways of B[a]P.

that escapes these detoxification reactions can enter the nucleus and react with genomic DNA to form a number of diastereomeric 2'-deoxyguanosine (dGuo)- and 2'-deoxyadenosine (dAdo)-adducts (Scheme 2).^{1,10,11}

A second pathway of metabolic activation involves aldo-keto reductase (AKR)-mediated oxidation of B[a]P-7,8-dihydrodiol to a ketol, which rearranges to an air-sensitive catechol (B[a]P-7,8-catechol).^{12,13,23} Interestingly, human AKR-1A1 stereoselectivity oxidizes the (–)-B[a]P-7,8-dihydrodiol enantiomer,²⁴ while AKR-1C1 to AKR-1C4 will oxidize both enantiomers.²⁵ The ability of other human AKRs (such as AKR-1B1 and AKR-1B10) to oxidize B[a]P-7,8-dihydrodiols has not been established. B[a]P-7,8-catechol undergoes two sequential one-electron autoxidation reactions to the *ortho*-quinone, B[a]P-7,8-dione, which has the potential to form DNA-adducts (Scheme 1).^{26–29} In the presence of cellular reducing equivalents, futile redox cycling occurs to produce reactive oxygen species (ROS) that can cause oxidative DNA damage.^{29,30} A third pathway of B[a]P activation has been identified, which involves the intermediate formation of a radical cation through the action of CYP peroxidases.^{31,32} It has been suggested that the B[a]P-radical cation can enter the nucleus, react with dGuo and dAdo residues in DNA, and finally undergo a second one-electron oxidation to form depurinating DNA-adducts (Scheme 1).¹⁴

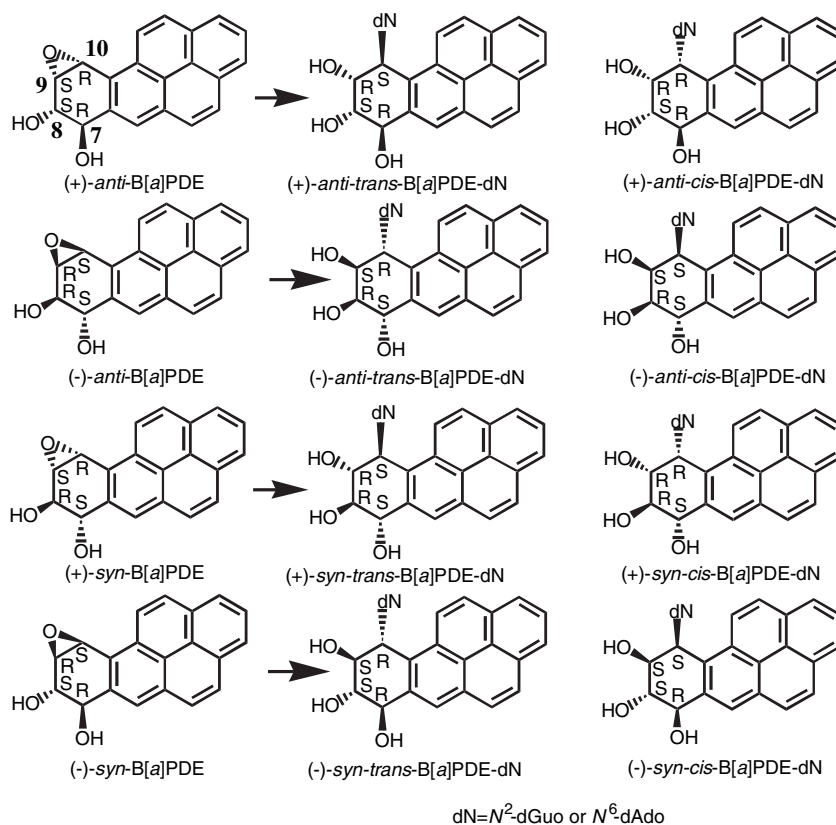
Two *anti* and two *syn* forms of B[a]PDE can arise from CYP-mediated B[a]P metabolism (Scheme 2). All four B[a]PDE diastereomers are mutagenic in bacterial and mammalian cell assays.^{33,34} However, (+)-*anti*-B[a]PDE is the most tumorigenic, causing pulmonary adenomas in mice.^{35–37} In order to determine the relative importance of the CYP-, AKR- and

radical-cation-mediated pathways of B[a]P metabolism (Scheme 1), we required a method to specifically quantify the (±)-*anti*-B[a]PDE-derived dGuo- and dAdo-adducts that are formed in DNA (Scheme 2). Previous studies of B[a]PDE-mediated DNA-adduct formation have relied heavily on non-specific methodology such as [³²P]-postlabeling,^{11,38} immunoassays,³⁸ and to a lesser extent fluorescence line broadening.³⁹ There are several reports on the analysis of B[a]P-adducts using more rigorous stable isotope dilution, mass spectrometry (MS)-based methodology^{40–43} or high sensitivity capillary electrophoresis/MS.⁴⁴ However, none of the previous methods have resolved the four dGuo- and four dAdo-adduct diastereomers that are formed from (±)-*anti*-B[a]PDE. We report the development and validation of a stable isotope dilution, liquid chromatography/tandem MS (LC/MS/MS) method using multiple reaction monitoring (MRM) that permits the quantitation of eight individual dGuo- and dAdo-adducts that arise in single- and double-stranded calf thymus DNA and in cellular DNA as a consequence of treatment with (±)-*anti*-B[a]PDE.

EXPERIMENTAL

Chemical and materials

Cell culture media and reagents were obtained from Invitrogen Co. (Carlsbad, CA, USA). Calf thymus DNA (ct-DNA), dAdo, dGuo, DNase, tetrahydrofuran (TFA), and triethylamine (TEA) were purchased from Sigma (St. Louis, MO, USA). [¹⁵N₅]-dGuo and [¹⁵N₅]-dAdo were obtained from Spectra Stable Isotopes (Columbia, MD, USA). Nuclease P1 and shrimp alkaline phosphatase (SAP) were purchased from Roche (Germany). (±)-*anti*-B[a]PDE was



Scheme 2. Stereochemistry of B[*a*]PDE- N^2 -dGuo and B[*a*]PDE- N^6 -dAdo adducts formed from (\pm)-*anti*-B[*a*]PDE and (\pm)-*syn*-B[*a*]PDE.

purchased from the NCI Chemical Carcinogen Standard Reference Repository (Midwest Research Institute, Kansas City, MO, USA). YMC ODS-AQ, Hypersil C18 and Chiralcel OD-RH high-performance liquid chromatography (HPLC) columns were obtained from Waters (Milford, MA, USA), Phenomenex (Torrance, CA, USA) and Chiral Technologies (West Chester, PA, USA), respectively. Costar spin-x nylon centrifuge filter tubes were purchased from Corning Inc. (Corning, NY, USA). HPLC-grade water, methanol, acetonitrile and ethanol were purchased from Optima, Fisher Scientific Co. (Fair Lawn, NJ, USA). Human bronchoalveolar adenocarcinoma H358 cells were obtained from the American Type Culture Collection (ATCC, Manassas, VA, USA; No. CRL-5807).

Synthesis of B[*a*]PDE-[15 N $_5$]- N^6 -dAdo adducts

A solution of (\pm)-*anti*-B[*a*]PDE (240 μ L; 16 mg/mL in THF containing 5% TEA) was added into a solution of [15 N $_5$]-dAdo (4 mg in 700 μ L of 0.5 M bis-Tris-HCl or 0.02 M phosphate buffer, pH 7.0) every 3 h, 60 μ L each time. The reaction was continued by stirring in the dark at 37°C for 72 h. Every 12 h, a portion of the reaction mixture (1 μ L) was transferred to 1 mL of 20% MeOH/H $_2$ O (v/v). The change in fluorescence intensity (excitation: 346 nm; emission: 400 nm) was monitored using a PerkinElmer LS-5 fluorescence detector (PerkinElmer Life and Analytical Sciences, Monza, Italy) before and after addition of 10 μ L 8 N HCl in order to detect the hydrolysis of any unreacted B[*a*]PDE. After the reaction was completed (72 h), the reaction mixture was evaporated under N $_2$ for 10 min to remove the THF.

Methanol (300 μ L) was added, and the reaction mixture was centrifuged at 14 000 rpm for 10 min. The precipitate was washed with 200 μ L of methanol/H $_2$ O (1:1, v/v) and centrifuged at 14 000 rpm for 10 min. The upper solution was combined with the supernatant from the reaction mixture. The combined solution was subjected to HPLC separation.

Synthesis of B[*a*]PDE-[15 N $_5$]- N^2 -dGuo adducts

A solution of (\pm)-*anti*-B[*a*]PDE (100 μ L; 10 mg/mL in dimethyl sulfoxide (DMSO)) was added into a solution of [15 N $_5$]-dGuo (1 mL; 10 mg/mL in 0.1 M Tris-HCl, pH 7.5). The reaction mixture was incubated in the dark at 37°C for 24 h and was extracted three times with 1 mL of butanol. The butanol layer was washed with 1 mL of H $_2$ O and evaporated to dryness under N $_2$. The dried mixture was dissolved in 500 μ L of DMSO/H $_2$ O (1:1, v/v) and subjected to HPLC separation.

Separation and purification of B[*a*]PDE-[15 N $_5$]- N^6 -dAdo and B[*a*]PDE-[15 N $_5$]- N^2 -dGuo adducts

Separation and purification of the adduct stereoisomers was performed using a Hitachi L7100 HPLC pump equipped with a Hitachi L7400 UV detector (Hitachi High-technologies, Tokyo, Japan). The primary separation was conducted on a preparative column (YMC ODS-AQ, 250 \times 10 mm, 5 μ m; Waters) using 20 mM TEA (pH 7.0) as mobile phase A, and acetonitrile as mobile phase B. The gradient started at 10% B and increased to 60% B in 50 min and continued to 100% B in 5 min at a flow rate of 3 mL/min. The peaks were fraction-

collected, combined, and the solvent was removed under vacuum using a Savant Speedvac concentrator. A secondary purification was conducted on an analytical column (Hypersil C18, 250 × 4.6 mm, 5 μm; Phenomenex) using 50 mM phosphate buffer (pH 7.0) as mobile phase A and methanol as mobile phase B at a flow rate of 1 mL/min. For B[a]PDE-[¹⁵N₅]-N⁶-dAdo adducts, the linear gradient was 50% B to 55% B over 50 min. For B[a]PDE-[¹⁵N₅]-N²-dGuo adducts, the linear gradient was 47% B to 51% B over 50 min. The first peak for B[a]PDE-[¹⁵N₅]-N²-dGuo was further separated by a chiral HPLC column (Chiracel OD-RH, 150 × 4.6 mm; Daicel, Tokyo, Japan) using water as mobile phase A and acetonitrile as mobile phase B at a flow rate of 1 mL/min. The gradient was 5% B to 10% B in 30 min, followed by 20% B in 10 min, and 20% B was held for another 10 min. Each peak was collected, and the solvent was removed under vacuum using a Speedvac concentrator. Desalting was conducted in a third purification step with the Hypersil C18 column described above using water as mobile phase A, and acetonitrile as mobile phase B. The gradient was 10% B for 5 min, followed by 10% B to 35% B in 30 min at a flow rate of 1 mL/min. Samples were dried under N₂ and dissolved in water. The purity of each purified adduct was confirmed by examination of its UV and circular dichroism (CD) spectra.

Synthesis, separation and purification of B[a]PDE-N⁶-dAdo and B[a]PDE-N²-dGuo adducts

A solution of (±)-*anti*-B[a]PDE (5 mg in 250 μL of THF containing 5% TEA) was reacted with dGuo or dAdo saturated in 1 mL of Tris-HCl (pH 7.0–7.5). The reaction conditions, separation and purification procedures were the same as described above for the isotope-labeled adducts.

Characterization and structure identification

UV and CD spectra (220–400 nm) of each adduct were measured on a Beckman Du530 UV/VIS spectrometer (Beckman Coulter, Inc., Fullerton, CA, USA) and Aviv 202 CD spectrometer (Aviv Biomedical, Lakewood NJ, USA), respectively. LC/MS/MS data were acquired on a Waters 2690 LC system with autosampler, Hitachi L-6000 UV/Vis detector, and Finnigan LCQ ion-trap mass spectrometer (Thermo, San Jose, CA, USA). The HPLC method employed the Hypersil C18 column described above using a 5 mM NH₄OAc buffer containing 0.02% formic acid as mobile phase A and methanol as mobile phase B at a flow rate of 1 mL/min. For B[a]PDE-[¹⁵N₅]-N⁶-dAdo adducts, the gradient was 0% B to 50% B in 10 min and continued to 55% B in 40 min. For B[a]PDE-[¹⁵N₅]-N²-dGuo adducts, the gradient was 0% B to 47% B in 10 min and continued to 54% B in 40 min. UV absorbance was monitored at 260 nm. The mass spectrometer was operated in the positive electrospray ionization (ESI) mode with a 4.5 kV spray voltage. The capillary temperature was held at 200°C. Sheath gas and auxiliary gas were set at 80 and 10 units, respectively. Collision-induced dissociation (CID) experiments coupled with multiple tandem mass spectrometry (MSⁿ) employed helium as the collision gas. The relative collision energy was set at 35% of the maximum (1 V). Activation time of the dependent scan was 30 ms.

DNA-adducts from calf thymus DNA

Ct-DNA (600 μg) was dissolved in 600 μL of 20 mM phosphate buffer, pH 7.0. Half of the solution (300 μL) was transferred to another tube and denatured at 95°C for 5 min. The denatured ct-DNA was quickly chilled at 0°C for 10 min and heated to 37°C. A solution of (±)-*anti*-B[a]PDE (0.4 mg in 150 μL of THF containing 5% TEA) was added into the native or denatured (single-stranded) ct-DNA solution. The reaction was conducted by stirring in the dark at 37°C for 3 days. After incubation, the reaction mixture was evaporated under a N₂ stream to reduce the volume to 200 μL; then the mixture was centrifuged at 14 000 rpm for 10 min. The supernatant was transferred to another tube. The residue was washed with 100 μL of 20 mM phosphate buffer (pH 7.0) and centrifuged at 14 000 rpm for 10 min. The washing solution was then combined with the supernatant (total volume 300 μL) to give the modified ct-DNA.

Culture of human bronchoalveolar H358 cells

The cells were maintained in RPMI 1640 medium with 10% fetal bovine serum, 1% L-glutamine and 100 units/mL of penicillin/streptomycin. The cells were incubated at 37°C in a humidified atmosphere of 5% CO₂ and were passaged at a dilution of 1:3 every 4 days.

Formation of DNA-adducts in human bronchoalveolar adenocarcinoma H358 cells and isolation of DNA

After the cells reached 70–80% confluence (approximately 1 × 10⁷ cells), the complete RPMI was removed and replaced with 10 mL HBSS buffer containing 20 μM of (±)-*anti*-B[a]PDE and 400 μM of β-cyclodextrin as a PAH carrier. The (±)-*anti*-B[a]PDE was dissolved in DMSO (5 mM) so that the final concentration of DMSO in the culture medium was <0.5%. Control cells were treated with HBSS buffer containing DMSO and β-cyclodextrin. The cells were incubated for 24 h, washed with phosphate-buffered saline (PBS) and collected by scraping. DNA from 1 × 10⁷ cells was extracted with a Wako DNA extraction kit (Wako Chemicals USA, Inc., Richmond, VA, USA) which employed sodium iodide as a chaotropic agent using the procedure described in the manufacturer's instructions. The DNA pellets were dried under N₂ and then dissolved in 300 μL of 20 mM phosphate buffer, pH 7.0.

DNA hydrolysis and purification of DNA-adducts

The solution containing ct-DNA (300 μL) or H358 cell DNA (300 μL) was subjected to enzyme hydrolysis by addition of 30 μL of 0.1 M MgCl₂ and 400 units of DNase I, followed by incubation for 1 h at 37°C. A solution (5 μL) of 50 mM NaOAc, 5 mM ZnCl₂, pH 5.0, was then added along with 7.5 units of nuclease P1, and the sample was incubated for 1.5 h at 37°C. At the end of the incubation, 40 μL of 0.5 M Tris-HCl, 50 mM MgCl₂, pH 8.5, was added along with 20 units of SAP, and the sample was incubated for a further 1.5 h at 37°C. An aliquot (50 μL) was taken for base analysis. B[a]PDE-[¹⁵N₅]-N⁶-dAdo (80 ng) and B[a]PDE-[¹⁵N₅]-N²-dGuo (200 ng) internal standards were then added. Ethanol (900 μL) was added into the digestion solution, and the sample was chilled at 0°C for 10 min. The sample was

centrifuged at 14 000 rpm for 10 min at 4°C. The clear solution was transferred to another tube and evaporated to a volume of 100 µL under a stream of N₂. To the solution was added 100 µL of methanol, which was then filtered through a Costar spin-x nylon centrifuge filter tube before analysis by LC/MS. The injection volume was 50 µL.

LC/MS conditions for DNA-adduct quantification

Data were acquired using an Agilent 1100 HPLC system (Agilent Technology, Palo Alto, CA, USA) equipped with CTC autosampler (Leap Technology, Carrboro, NC, USA) coupled to an MDS-Sciex API-4000 triple-quadrupole mass spectrometer (Applied Biosystems, Foster City, CA, USA). The HPLC method employed a YMC ODS-AQ column (150 × 2.0 mm, 5 µm) using a 5 mM NH₄OAc buffer containing 0.02% formic acid as mobile phase A and methanol as mobile phase B at a flow rate of 250 µL/min. The linear gradient started from 49% B to 51% B in 20 min, followed by 51% B to 65% B in 10 min and continued to 100% B in 5 min. The mass spectrometer parameters were as follows: curtain gas at 15 units; gas-1 at 30 units; gas-2 at 10 units; ion spray voltage at 5.5 kV; ionization temperature at 450°C; CID gas at 10 units; decluster potential at 85 V; entrance potential at 10 V; collision energy at 47 eV; collision cell exit potential at 32 V. MRM analyses were conducted in the positive ESI mode using the following mass transitions: m/z 570.2 (MH⁺, B[*a*]PDE-*N*²-dGuo) → m/z 257.1 (MH⁺-dGuo-H₂O-CO); m/z 575.2 (B[*a*]PDE-[¹⁵N₅]-*N*²-dGuo) → m/z 257.1 (MH⁺-[¹⁵N₅]-dGuo-H₂O-CO); m/z 554.2 (MH⁺, B[*a*]PDE-*N*⁶-dAdo) → m/z 257.1 (MH⁺-dAdo-H₂O-CO); m/z 559.2 (MH⁺, B[*a*]PDE-[¹⁵N₅]-*N*⁶-dAdo) → m/z 257.1 (MH⁺-[¹⁵N₅]-dAdo-H₂O-CO).

Quantification and quality control for DNA-adducts

Concentrations of authentic standard solutions were confirmed from intensities of the characteristic absorbance maxima and known extinction coefficients in the 320–350 nm range.⁴⁵ Calibration curves for the DNA-adducts were prepared using authentic samples of the four stereoisomers of authentic B[*a*]PDE-*N*⁶-dAdo (0, 1.0, 2.0, 5.0, 10.0, 25, 50, 100 ng of each) and the four stereoisomers of authentic B[*a*]PDE-*N*²-dGuo (0, 1.0, 2.0, 5.0, 10.0, 25, 50, 100 ng of each). Also, 80 ng of B[*a*]PDE-[¹⁵N₅]-*N*⁶-dAdo and 200 ng of B[*a*]PDE-[¹⁵N₅]-*N*²-dGuo were spiked into 300 µL of digested ct-DNA solution. Standard solutions underwent the same sample preparation and analytical procedures as the unknown samples. Calibration curves were calculated by linear regression analysis of peak area ratios of analyte to internal standard plotted against amount of authentic analyte. DNA-adduct levels were calculated by interpolation from the calibration curve and normalized against the total base content in each sample. Quality control samples were prepared in triplicate by spiking 300 µL of digested ct-DNA solution with authentic standards (2.0, 10 and 50 ng of each stereoisomer, 3×) and internal standards (80 ng of B[*a*]PDE-[¹⁵N₅]-*N*⁶-dAdo and 200 ng of B[*a*]PDE-[¹⁵N₅]-*N*²-dGuo). The quality control samples underwent the same sample preparation and analytical procedures as the unknown samples.

DNA base analysis

LC-UV chromatography for DNA base analysis was conducted on a Hitachi Elite Lachrom HPLC system equipped with a UV detector. The separation employed a Phenomenex Jupiter C18 column (250 × 4.6 mm, 5 µm). Solvent A was water, and solvent B was acetonitrile. The flow rate was 1.0 mL/min, and the gradient was as follows: 0% B for 5 min followed by 5% B to 8% B for 20 min. The UV detector monitored the absorbance at 260 nm. For calibration curves, solutions containing different concentrations of authentic DNA bases (0, 2.0, 5.0, 10.0, 20.0, 50.0 µg/mL) were subjected to HPLC analysis. Injection volume was 20 µL. Calibration curves were calculated with a linear regression analysis of the peak areas of authentic standards. A portion of the digested sample was subjected to the same HPLC procedure for base analysis. DNA base levels were calculated by interpolation from the calibration curve.

RESULTS

Synthesis and characterization of B[*a*]PDE-[¹⁵N₅]-*N*⁶-dAdo and B[*a*]PDE-[¹⁵N₅]-*N*²-dGuo stereoisomers

[¹⁵N₅]-labeled (±)-*anti*-B[*a*]PDE-*N*⁶-dAdo and *N*²-dGuo adduct standards were chemically synthesized. A reversed-phase HPLC method was developed for fast separation of all the adduct stereoisomers. For synthesis of B[*a*]PDE-[¹⁵N₅]-*N*²-dGuo adducts, the abundance of each stereoisomer was well balanced (16% reaction yield, each stereoisomer accounted for 23–30% of the total adducts formed). The adducts were first separated by preparative reversed-phase HPLC from unreacted dGuo and hydrolyzed B[*a*]PDE. The adduct fraction was further purified by analytical reversed-phase HPLC and separated into three different elution fractions, denoted by B[*a*]PDE-[¹⁵N₅]-*N*²-dGuo adduct G1 (retention time 29.5 min), G2 (retention time 30.1 min), and G3 (retention time 33.1 min) (Fig. 1(A)). Fraction G1 was further subjected to a chiral HPLC separation that resulted in fractions containing adduct G1a and G1b (Fig. 1(B)).

B[*a*]PDE was less reactive to dAdo than dGuo. Different conditions were used to synthesize B[*a*]PDE-*N*⁶-dAdo, and the reaction yields were compared. In phosphate buffer, the reaction favored *cis* addition of B[*a*]P moiety to the mononucleoside, and less *trans* adducts were formed than *cis* adducts (10–12% reaction yield, 5–10% *trans* stereoisomers of the total adducts formed). In Tris buffer, the reaction yield improved to 12–16%, but even smaller amounts of the *trans* addition adducts were generated (1–2% *trans* stereoisomers of the total adducts formed). Both conditions were used for preparation of the B[*a*]PDE-[¹⁵N₅]-*N*⁶-dAdo adducts. The adduct mixture was collected after the primary preparative HPLC purification. The fraction of B[*a*]PDE-[¹⁵N₅]-*N*⁶-dAdo adducts was subjected to further analytical HPLC separation. Four major adducts were then obtained and labeled as B[*a*]PDE-[¹⁵N₅]-*N*⁶-dAdo adduct A1 (retention time 30.5 min), A2 (retention time 32.2 min), A3 (retention time 34.3 min), and A4 (retention time 36.8 min) (Fig. 2(A)).

The structure and stereochemistry of the adduct stereoisomers were determined by a combination of LC-MS, UV, and CD spectroscopy. These adducts were subjected to MS

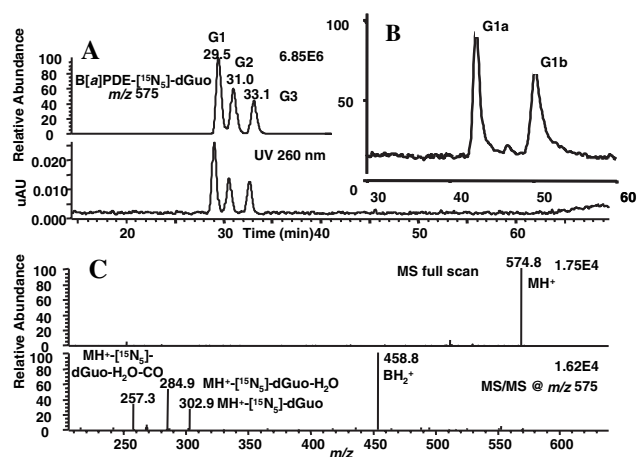


Figure 1. (A) LC-MS/UV analysis of the stereoisomers of B[a]PDE-[¹⁵N₅]-N²-dGuo adducts. Upper panel: ion chromatogram for MH⁺ (*m/z* 575); lower panel: UV absorbance at 260 nm. (B) LC/MS analysis of the B[a]PDE-[¹⁵N₅]-N²-dGuo adduct G1, which is separated as G1a and G1b on a chiral column. (C) Mass spectra of B[a]PDE-[¹⁵N₅]-N²-dGuo adduct G2. Upper panel: mass spectrum; lower panel: MS² spectrum. The other three adducts had mass spectra that were identical.

and MS² analysis for structure confirmation. All of the four B[a]PDE-[¹⁵N₅]-N²-dGuo adducts showed a MH⁺ at *m/z* 575 (Fig. 1(C)). MS² analysis of *m/z* 575 resulted in the formation of fragments at *m/z* 459, 303, 285, and 257 (Fig. 1(C)). The fragment ion at *m/z* 459 corresponded to the protonated modified base (B) to which an additional proton had been transferred (BH₂⁺) (Scheme 3(A)). The fragment ion at

m/z 303 corresponded to MH⁺ with loss of [¹⁵N₅]-dGuo, which further dehydrated into the fragment ion at *m/z* 285. Loss of the CO group from *m/z* 285 gave rise to *m/z* 257. All of the four B[a]PDE-[¹⁵N₅]-N⁶-dAdo adducts showed a MH⁺ at *m/z* 559 (Fig. 2(B)). MS² analysis of *m/z* 559 resulted in the formation of fragments at *m/z* 443, 303, 285, and 257 (Fig. 2(B)). The fragment ion at *m/z* 443 corresponded to the protonated modified base (B) to which an additional proton had been transferred (BH₂⁺) (Scheme 3(B)). The fragment ion at *m/z* 303 corresponded to MH⁺ with loss of [¹⁵N₅]-dAdo, which further dehydrated into the fragment ion at *m/z* 285. Loss of the CO group from *m/z* 285 gave rise to *m/z* 257.

UV and CD spectra were obtained to identify the stereochemistry of each adduct. The adducts were classified into two groups by absorbance at 320–350 nm, which is the characteristic range for the aromatic ring system of B[a]PDE. One group of adducts (group 1),^{46,47} B[a]PDE-[¹⁵N₅]-N²-dGuo adducts G1b and G2 and B[a]PDE-[¹⁵N₅]-N⁶-dAdo adducts A2 and A4, exhibited a characteristic absorbance maximum at 346 nm, while the other group (group 2),^{46,47} B[a]PDE-[¹⁵N₅]-N²-dGuo adducts G1a and G3 and B[a]PDE-[¹⁵N₅]-N⁶-dAdo adducts A1 and A3, exhibited a maximum absorbance at shorter wavelength (345 nm). Since the B[a]PDE-monomucleoside adducts in the *cis* configuration showed a stronger red-shift than those in *trans* configuration, group 1 adducts were assigned as *cis* stereoisomers, and group 2 adducts were assigned as *trans* stereoisomers. The CD spectrum of each adduct is shown in Fig. 3. Each pair of diastereomeric adducts exhibited similar CD spectra that were opposite in sign. B[a]PDE adducts having a 10S

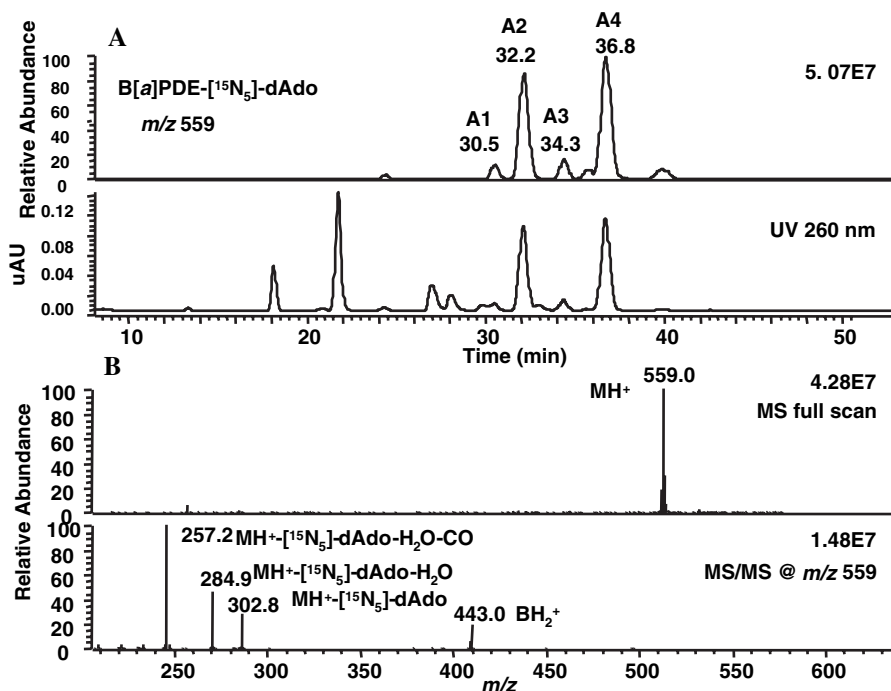
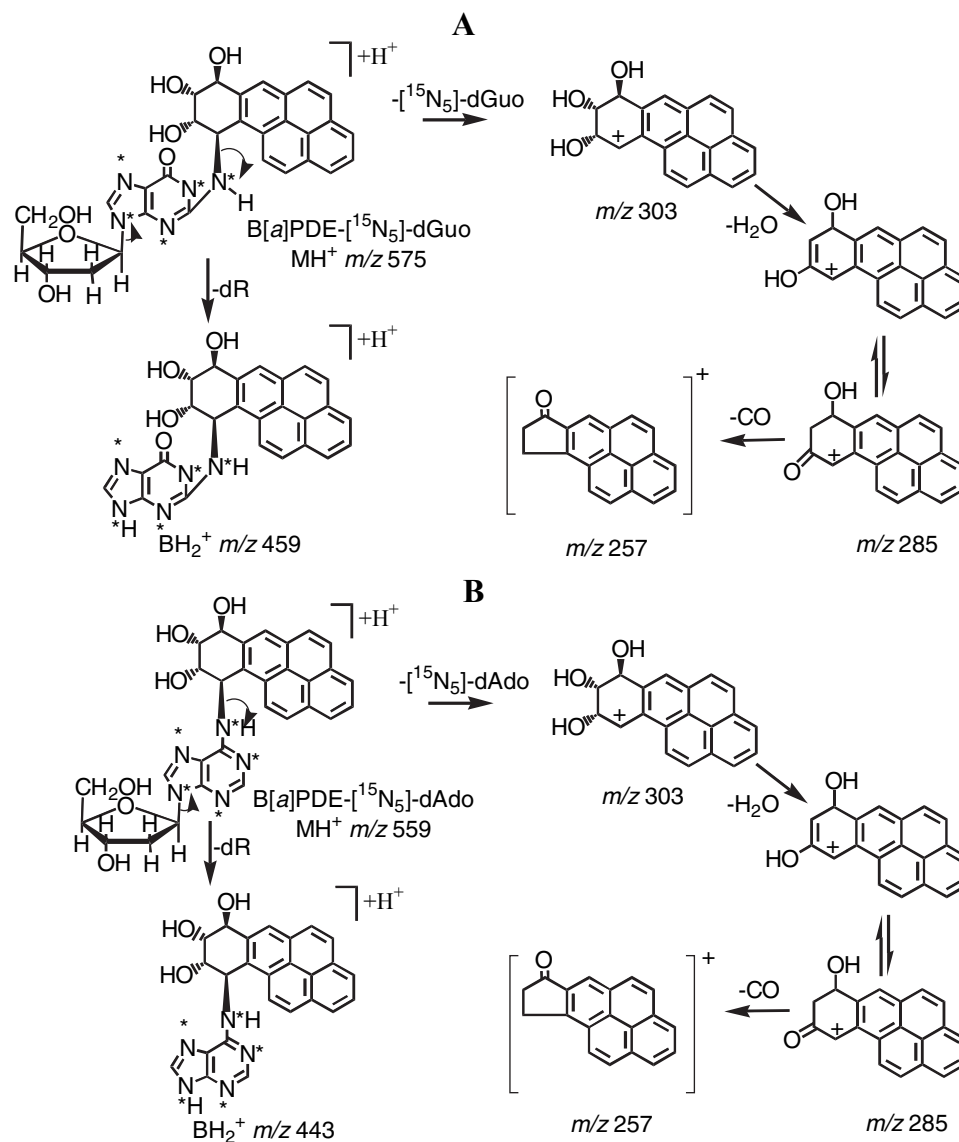


Figure 2. (A) LC-MS/UV analysis of the stereoisomers of B[a]PDE-[¹⁵N₅]-N⁶-dAdo adducts. Upper panel: ion chromatogram for MH⁺ (*m/z* 559); lower panel: UV absorbance at 260 nm. (B) Mass spectra of B[a]PDE-[¹⁵N₅]-N⁶-dAdo adduct A1. Upper panel: mass spectrum; lower panel: MS² spectrum. The other three adducts had mass spectra that were identical.



Scheme 3. Pathways for formation of product ions from CID of MH^+ : (A) B[a]PDE-[$^{15}N_5$]- N^2 -dGuo adducts and (B) B[a]PDE-[$^{15}N_5$]- N^6 -dAdo adducts.

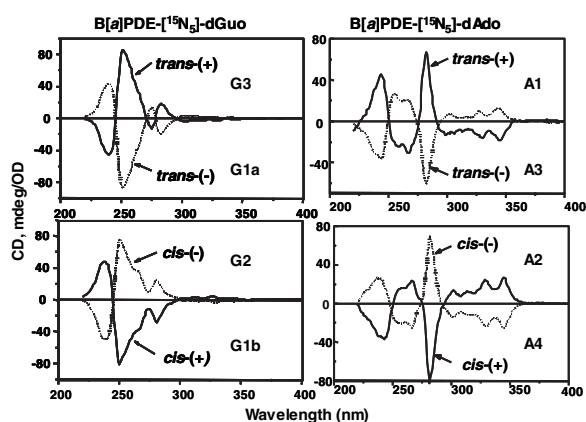


Figure 3. CD spectra of stereoisomers of B[a]PDE-[$^{15}N_5$]- N^2 -dGuo and B[a]PDE-[$^{15}N_5$]- N^6 -dAdo adducts. Left panels: CD spectra of B[a]PDE- N^2 -dGuo adducts; right panels: CD spectra of B[a]PDE- N^6 -dAdo adducts.

absolute configuration, which corresponded to (+)-*trans* or (–)-*cis*, each exhibited a positive signal for their most intense CD band.^{48,49} Adducts having a 10*R* absolute configuration, which corresponded to (–)-*trans* or (+)-*cis*, each exhibited a negative signal for their most intense CD band.^{48,49} The unlabeled adducts shared identical UV and CD characteristics with the corresponding labeled analogues. The B[a]PDE-[$^{15}N_5$]- N^2 -dGuo adducts G1a, G1b, G2, and G3 were assigned as (–)-*trans*, (+)-*cis*, (–)-*cis*, and (+)-*trans*-stereoisomers, respectively. The B[a]PDE-[$^{15}N_5$]- N^6 -dAdo adducts A1, A2, A3, and A4 were assigned as (+)-*trans*-, (–)-*cis*-, (–)-*trans*-, and (+)-*cis*-stereoisomers, respectively.

Development of a stable isotope dilution LC/MS/MS method for quantitation of B[a]PDE- N^2 -dGuo and B[a]PDE- N^6 -dAdo adducts

In order to develop a quantitation method, unlabeled B[a]PDE- N^2 -dGuo and B[a]PDE- N^6 -dAdo authentic standards

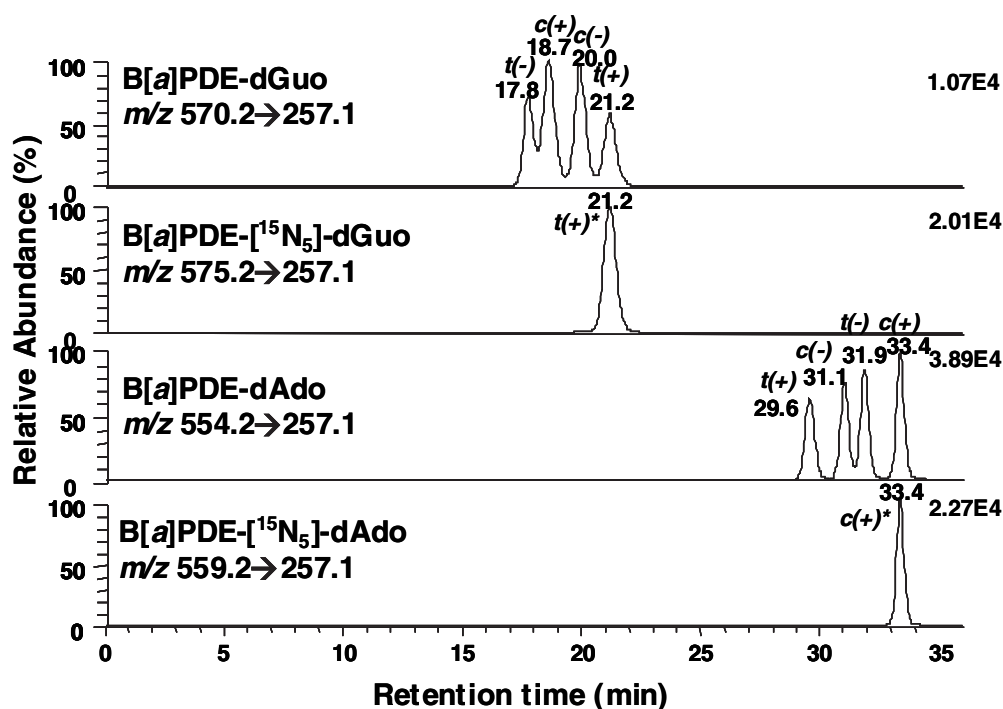


Figure 4. Stable isotope dilution LC-MRM/ESI-MS analysis of standard B[a]PDE- N^2 -dGuo and B[a]PDE- N^6 -dAdo adducts. MRM chromatograms are shown for: B[a]PDE- N^2 -dGuo (m/z 570.2 \rightarrow 257.1), B[a]PDE- $^{15}\text{N}_5$ - N^2 -dGuo (m/z 575.2 \rightarrow 257.1), B[a]PDE- N^6 -dAdo (m/z 554.2 \rightarrow 257.1), and B[a]PDE- $^{15}\text{N}_5$ - N^6 -dAdo (m/z 559.2 \rightarrow 257.1).

were chemically synthesized and characterized with the same procedure as that used for stable-isotope-labeled adducts. An HPLC method was developed to separate all four B[a]PDE- N^2 -dGuo and four B[a]PDE- N^6 -dAdo stereoisomers in 35 min by a reversed-phase C18 column with hydrophilic end-capping (Fig. 4). The column size was optimized to 150×2.0 mm to accommodate a lower flow rate ($250 \mu\text{L}/\text{min}$) for ESI, which made the analysis possible without using a splitter that would have decreased sensitivity.

For quantitation of B[a]PDE- N^2 -dGuo adducts, the B[a]PDE- $^{15}\text{N}_5$ - N^2 -dGuo adduct G3 [(+)-*trans*] was added as the internal standard. For quantitation of B[a]PDE- N^6 -dAdo adducts, the B[a]PDE- $^{15}\text{N}_5$ - N^6 -dAdo adduct A4 [(+)-*cis*] was added as the internal standard (Fig. 4). The following specific MRM transitions were monitored for the adducts: m/z 570.2 [MH^+] to m/z 257.1 [MH^+ -dGuo- H_2O -CO] for B[a]PDE- N^2 -dGuo adducts; m/z 575.2 [MH^+] to m/z 257.1 [MH^+ -dGuo- H_2O -CO] for B[a]PDE- N^2 -dGuo internal standard; m/z 554.2 [MH^+] to m/z 257.1 [MH^+ -dAdo- H_2O -CO] for B[a]PDE- N^6 -dAdo adducts; and m/z 559.2 [MH^+] to m/z 257.1 [MH^+ - $^{15}\text{N}_5$ -dAdo- H_2O -CO] for B[a]PDE- N^6 -dAdo (internal standard).

Retention times for the four B[a]PDE- N^2 -dGuo adducts were 17.8 min [(−)-*trans*], 18.7 min [(+)-*cis*], 20.0 min [(−)-*cis*], and 21.2 min [(+)-*trans*] (Fig. 4). B[a]PDE- $^{15}\text{N}_5$ - N^2 -dGuo internal standard [(+)-*trans*] eluted at 21.2 min. The retention times for the four B[a]PDE- N^6 -dAdo adducts were 29.6 min [(+)-*trans*], 31.1 min [(−)-*cis*], 31.9 min [(−)-*trans*], and 33.4 min [(+)-*cis*]. The B[a]PDE- $^{15}\text{N}_5$ - N^6 -dAdo internal standard [(+)-*cis*] eluted at 33.4 min.

Calibration curves (range from 4.3–430 ng/mL) were constructed for the four B[a]PDE- N^2 -dGuo adducts (Fig. 5(A)) and

the four B[a]PDE- N^6 -dAdo adducts (Fig. 5(B)). High linearity was achieved for all the adducts ($r^2 > 0.997$ for B[a]PDE- N^2 -dGuo adducts and $r^2 > 0.9995$ for B[a]PDE- N^6 -dAdo adducts). The detection limits for B[a]PDE- N^2 -dGuo and B[a]PDE- N^6 -dAdo adducts were 10 pg and 5 pg on-column, respectively. Triplicate quality control samples (HQC, MQC and LQC $\times 3$) were used to evaluate accuracy and precision of the quantification method. The error of all the quality control samples was within the range of $\pm 10\%$ (Table 1).

Quantitation of dGuo- and dAdo-adducts in ct-DNA treated with B[a]PDE

Double- and single-stranded forms of ct-DNA were reacted with (\pm)-*anti*-B[a]PDE and subjected to enzyme hydrolysis, followed by LC/MS/MS quantitation of B[a]PDE- N^2 -dGuo and B[a]PDE- N^6 -dAdo adducts. The total amounts of adducts in double- and single-stranded DNA after the reaction were similar. There were 0.90 ± 0.20 and 0.94 ± 0.16 adducts/ 10^3 normal bases in double-stranded DNA and single-stranded DNA, respectively. The major B[a]PDE- N^2 -dGuo adduct formed in the reaction between native ct-DNA (double stranded) and (\pm)-*anti*-B[a]PDE was (+)-*trans*-B[a]PDE- N^2 -dGuo, and the minor adduct was the (−)-*trans*-B[a]PDE- N^2 -dGuo stereoisomer (Fig. 6). The major B[a]PDE- N^6 -dAdo adducts were (+)-*cis*-B[a]PDE- N^6 -dAdo, followed by (−)-*trans*-, (−)-*cis*-, and (+)-*trans*-B[a]PDE- N^6 -dAdo (Fig. 6). Quantitation showed that B[a]PDE- N^2 -dGuo adducts were produced at a level of 10^3 adducts/ 10^6 normal bases (Fig. 7(A)). The most abundant adduct, (+)-*trans*-B[a]PDE- N^2 -dGuo, was 83.2% of the total B[a]PDE- N^2 -dGuo adducts (820 ± 260 adducts/ 10^6 normal bases). The amount of (−)-*trans*-B[a]PDE- N^2 -dGuo was 14.9% of the total B[a]PDE- N^2 -dGuo

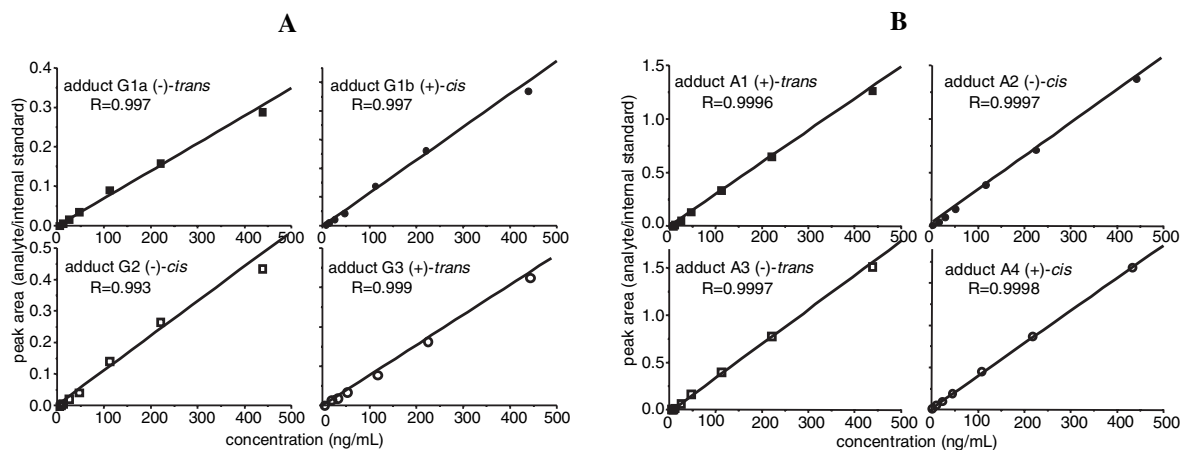


Figure 5. Calibration curves for (A) B[*a*]PDE-*N*²-dGuo adducts and (B) B[*a*]PDE-*N*⁶-dAdo adducts.

Table 1. Precision and accuracy for the determination of B[*a*]PDE-*N*⁶-dAdo and B[*a*]PDE-*N*²-dGuo adducts

Compound		Parameter	LQC (n = 3)	MQC (n = 3)	HQC (n = 3)
B[<i>a</i>]PDE- <i>N</i> ⁶ -dAdo	<i>t</i> (-)	Theoretical (ng/mL)	8.60	43.0	215
		Mean (ng/mL)	8.36	43.5	200
		RSD (%)	0.6	2.6	1.8
		Accuracy (%)	97.2	101	93
	<i>c</i> (+)	Mean (ng/mL)	8.77	44.1	208
		RSD (%)	0.9	0.6	1.3
		Accuracy (%)	102	103	97
	<i>c</i> (-)	Mean (ng/mL)	8.56	43.5	207
		RSD (%)	4.8	1.8	0.8
		Accuracy (%)	99.5	101	96
	<i>t</i> (+)	Mean (ng/mL)	8.87	44.9	212
		RSD (%)	1.6	1.5	2.2
Accuracy (%)		103	104	99	
B[<i>a</i>]PDE- <i>N</i> ² -dGuo	<i>t</i> (+)	Mean (ng/mL)	8.03	44.4	217
		RSD (%)	2.6	1.2	2.2
		Accuracy (%)	93.3	103	101
	<i>c</i> (-)	Mean (ng/mL)	8.00	42.5	217
		RSD (%)	0.5	1.3	1.7
		Accuracy (%)	93.0	98.9	101
	<i>t</i> (-)	Mean (ng/mL)	8.16	44.3	222
		RSD (%)	0.3	1.0	1.2
		Accuracy (%)	94.8	103	103
	<i>c</i> (+)	Mean (ng/mL)	8.28	44.1	218
		RSD (%)	1.6	0.6	1.0
		Accuracy (%)	96.3	103	101

adducts (147 ± 51 adducts/ 10^6 normal bases). (+)-*cis*- and (-)-*cis*-B[*a*]PDE-*N*²-dGuo were detected at very low levels and only accounted for 1.1% (11.1 ± 0.7 adducts/ 10^6 normal bases) and 0.8% (7.4 ± 4.8 adducts/ 10^6 normal bases) of the total B[*a*]PDE-*N*²-dGuo adducts, respectively. B[*a*]PDE-*N*⁶-dAdo adducts were formed at approximately 2 orders of magnitude lower than those of B[*a*]PDE-*N*²-dGuo adducts (Fig. 7(B)). The most abundant adduct, (+)-*cis*-B[*a*]PDE-*N*⁶-dAdo, was present at 11.0 ± 4.2 adducts/ 10^6 normal bases (44.4% of the total B[*a*]PDE-*N*⁶-dAdo adducts). (-)-*trans* and (-)-*cis*-B[*a*]PDE-*N*⁶-dAdo were present in similar amounts and were detected at 5.5 ± 1.6 adducts/ 10^6 normal bases (22.0% of the total B[*a*]PDE-*N*⁶-dAdo adducts) and 5.1 ± 3.5 adducts/ 10^6 normal bases (20.4% of the total B[*a*]PDE-*N*⁶-dAdo adducts), respectively. (+)-*trans*-B[*a*]PDE-*N*⁶-dAdo accounted for only 13.2% of the B[*a*]PDE-*N*⁶-dAdo adducts

(3.3 ± 1.2 adducts/ 10^6 normal bases). In total, 97.5% of all the adducts detected were B[*a*]PDE-*N*²-dGuo adducts, and 2.5% were B[*a*]PDE-*N*⁶-dAdo adducts.

Reaction of denatured (single-stranded) ct-DNA with B[*a*]PDE gave slightly different relative abundances of the different stereoisomers when compared with double-stranded ct-DNA. The amounts of (+)-*trans*-, (-)-*trans*-, (+)-*cis*- and (-)-*cis*-B[*a*]PDE-*N*²-dGuo adducts were 575 ± 70 (60.0%), 350 ± 27 (36.6%), 20.1 ± 1.7 (2.1%), and 12.8 ± 0.7 (1.3%) adducts/ 10^6 normal bases, respectively (Fig. 7(C)). Therefore, significantly more of the (-)-*trans*-B[*a*]PDE-*N*²-dGuo adduct was formed than with double-stranded DNA (Fig. 7(A)). The amounts of (+)-*cis*-, (-)-*cis*-, (-)-*trans*- and (+)-*trans*-B[*a*]PDE-*N*⁶-dAdo adducts were 20.6 ± 1.0 (47.5%), 10.6 ± 0.6 (24.5%), 8.8 ± 0.4 (20.4%), and 3.3 ± 0.2 (7.7%) adducts/ 10^6 normal bases, respectively (Fig. 7(D)). In total,

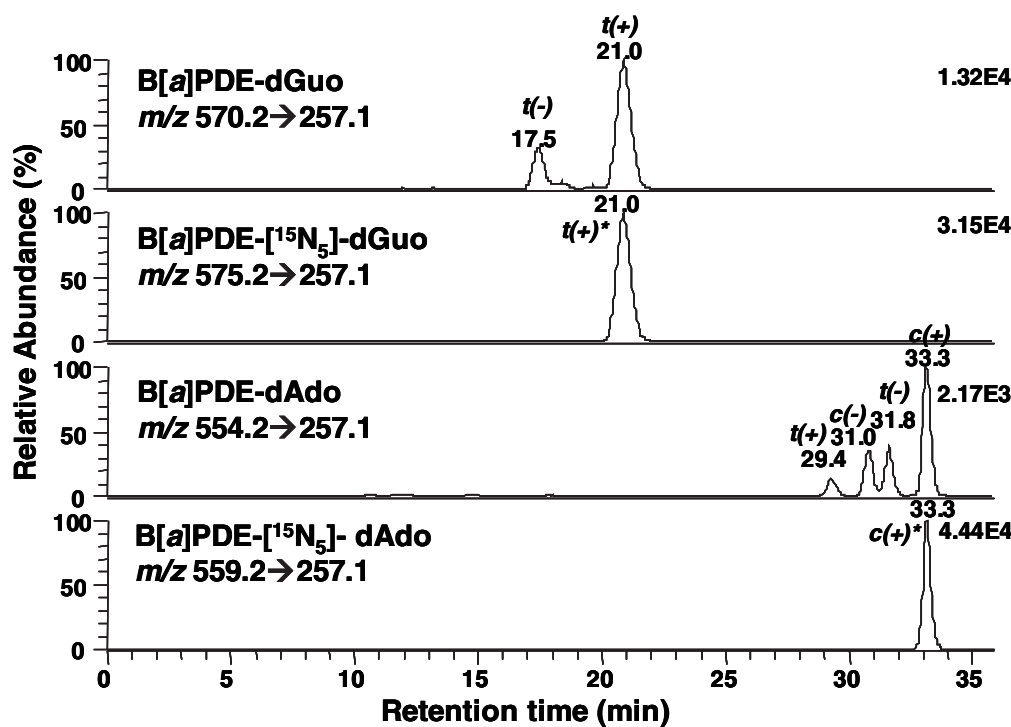


Figure 6. Representative chromatograms of stable isotope dilution LC-MRM/ESI-MS analysis of B[a]PDE- N^2 -dGuo and B[a]PDE- N^6 -dAdo adducts in double-stranded ct-DNA treated with B[a]PDE for 72 h at 37°C. Legends are the same as for Fig. 4.

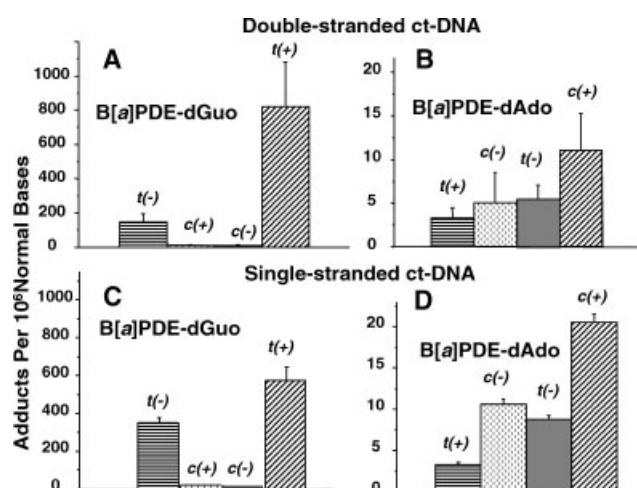


Figure 7. Amounts of B[a]PDE- N^2 -dGuo and B[a]PDE- N^6 -dAdo adducts in double-stranded ct-DNA (A, B) or single-stranded ct-DNA (C, D) treated with B[a]PDE for 72 h at 37°C. Analyses were performed by stable isotope dilution LC-MRM/ESI-MS. Determinations were conducted in triplicate (means \pm SD).

B[a]PDE- N^2 -dGuo adducts accounted for 95.7% and B[a]PDE- N^6 -dAdo adducts accounted for 4.3% of all the B[a]PDE adducts detected.

Quantitation of dGuo- and dAdo-adducts in the DNA of bronchoalveolar adenocarcinoma H358 cells treated with B[a]PDE

In the H358 cells treated with 20 μ M (\pm)-anti-B[a]PDE, the amounts of (+)-*trans*-, (-)-*trans*-, (+)-*cis*- and (-)-*cis*-B[a]PDE- N^2 -dGuo adducts were 331.7 ± 55 (88.3%),

27.2 ± 9.2 (7.2%), 12.3 ± 1.3 (3.3%), and 4.3 ± 0.9 (1.1%) adducts/ 10^6 normal bases, respectively ($n = 3$). The amounts of (+)-*cis*-, (-)-*cis*-, (-)-*trans*- and (+)-*trans*-B[a]PDE- N^6 -dAdo adducts were 0.35 ± 0.17 (25.9%), 0.21 ± 0.09 (15.5%), 0.53 ± 0.13 (39.4%), and 0.26 ± 0.01 (19.2%) adducts/ 10^6 normal bases, respectively ($n = 3$). In total, B[a]PDE- N^2 -dGuo adducts accounted for 99.6% and B[a]PDE- N^6 -dAdo adducts accounted for 0.4% of all the B[a]PDE adducts detected. Therefore, the predominant isomer was the (+)-*trans*-B[a]PDE-dGuo adduct. The H358 cells exhibited higher structural selectivity in adduct formation (Fig. 8) than ct-DNA (Fig. 6).

DISCUSSION

CYP-mediated metabolism of B[a]P results in the formation of B[a]PDE with high regioselectivity (Scheme 1).¹ The four resulting optical isomers can all potentially bind to DNA (Scheme 2), although there are substantial differences in mutagenicity of the individual isomers. In Chinese hamster V79 cells, (+)-*anti*-B[a]PDE was the most mutagenic, whereas (-)-*syn*-B[a]PDE was more mutagenic in the Ames test.³³ The incidence of pulmonary tumors in newborn mice treated with low doses of B[a]PDE isomers revealed that (+)-*anti*-B[a]PDE was by far the most potent tumorigen.³⁵ Similarly, (+)-*anti*-B[a]PDE was a more potent initiator of mouse skin tumorigenesis than (-)-*anti*-B[a]PDE.⁵⁰ Also, four diastereomers of *anti*-B[a]PDE- N^2 -dGuo and four diastereomers of *anti*-B[a]PDE- N^6 -dAdo can potentially be formed from the interaction of (+)- and (-)-*anti*-B[a]PDE with DNA (Scheme 2). This suggested that specific and sensitive methodology was required for analysis of DNA-adducts derived from the two *anti*-B[a]PDE enantiomers.

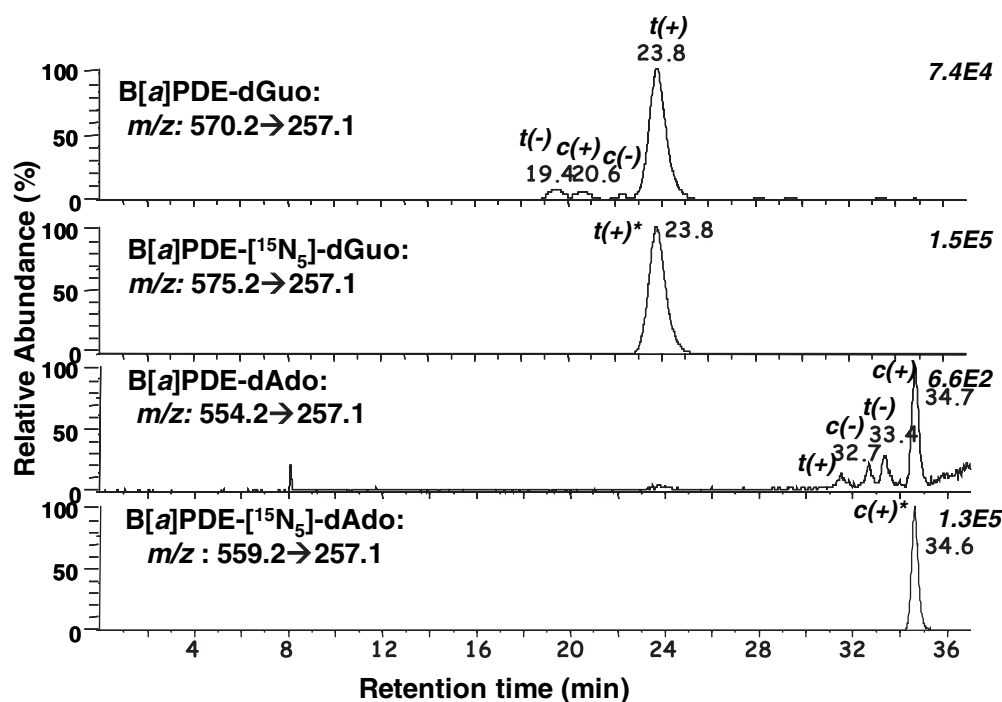


Figure 8. LC-MRM/MS analysis of B[a]PDE- N^2 -dGuo and B[a]PDE- N^6 -dAdo adducts in the DNA of H358 bronchoalveolar cells after treatment for 24 h with 20 μ M B[a]PDE. Legends are the same as for Fig. 4.

We have developed a stable isotope dilution LC-MRM/MS assay for all eight (\pm)-*anti*-B[a]PDE-derived DNA-adducts. This has made it possible to compare the relative and absolute amounts of each adduct that were formed in naked single- and double-stranded DNA treated with *anti*-B[a]PDE as well as DNA isolated from H358 cells treated with *anti*-B[a]PDE. There were 0.90 ± 0.20 and 0.94 ± 0.16 adducts/ 10^3 normal bases in double- and single-stranded DNA, respectively. The *anti*-B[a]PDE- N^2 -dGuo adducts were present in two orders of magnitude higher concentration than the *anti*-B[a]PDE N^6 -dAdo adducts in both naked and cellular DNA (Figs. 7 and 8). Therefore, dGuo residues are much more important targets for B[a]PDE than dAdo residues. Furthermore, the major adduct formed in both single- and double-stranded DNA was the dGuo adduct derived from (+)-*anti*-B[a]PDE (Fig. 7). Thus, (+)-*anti*-B[a]PDE binds at sites that facilitate covalent binding to dGuo residues in DNA.⁵¹

There was an even greater increased selectivity of (+)-*anti*-B[a]PDE for formation of dGuo-adducts in H358 cells than naked DNA (Fig. 8). This suggests that the (-)-*anti*-B[a]PDE enantiomer is more rapidly detoxified than the (+)-enantiomer through formation of tetrols^{13,21} and/or GSH-adducts;^{1,22} alternatively, the (-)-*anti-trans*-B[a]PDE-dGuo adduct may be more readily repaired. Although, it was demonstrated that (+)- and (-)-*anti-trans*-B[a]PDE-dGuo were repaired equally well by mammalian nucleotide excision repair *in vitro*.⁵² A recent study with A539 human epithelial lung carcinoma cells examined the relative amounts of BPDE-derived dGuo-adducts and dAdo-adducts using HPLC-fluorescence-based methodology.⁵³ Similar results were obtained as in the present study, although the amount of B[a]PDE used was significantly lower (1 μ M compared with 20 μ M). However, the adducts appeared to

be repaired more rapidly (through nucleotide excision repair) in the A549 cells when compared with the H358 cells that were used in the present study.

It is noteworthy that the (+)-*anti-trans*-B[a]PDE-dGuo adduct is highly mutagenic in mammalian cells.⁵⁴ Our confirmation that (+)-*anti-trans*-B[a]PDE-dGuo is the predominant adduct in the DNA of mammalian cells treated with (\pm)-B[a]PDE provides additional evidence that it is responsible for the observed tumorigenic effects of (+)-*anti*-B[a]PDE in mouse skin⁵⁰ and mouse lung.³⁵ Interestingly, (-)-B[a]P-7,8-dihydrodiol (the precursor of (+)-*anti*-B[a]PDE) was the predominant enantiomer formed from incubations of B[a]P with rat liver microsomes.⁵⁵ The enantiomeric excess of (-)-B[a]P-7,8-dihydrodiol over (+)-B[a]P-7,8-dihydrodiol from B[a]P incubations with rat liver microsomes was 86% for control rats, 84% for phenobarbital-induced rats, and 92% for 3-methylcholanthrene-induced rats. In addition, (+)-*anti*-B[a]PDE was the major B[a]PDE enantiomer formed when (-)-B[a]P-7,8-dihydrodiol was incubated with both control and induced rat liver microsomes.⁵⁵ If similar stereoselectivities are observed for metabolism of B[a]P and B[a]P-7,8-dihydrodiol by the CYPs present in cells from extrahepatic tissues, then there could be an even greater preference for formation of the (+)-*anti-trans*-B[a]PDE-dGuo adduct than was observed in incubations of (\pm)-*anti*-B[a]PDE with the H358 cells.

The H358 cells do not constitutively express CYP1A1 and CYP1B1 or AKR1A1 and AKR1C1 to AKR1C4.¹³ Up-regulation of the CYPs and/or transfection of the H358 cells with relevant AKRs provide model systems in which the two pathways of B[a]P activation can be modulated.⁵⁶ The availability of a stable isotope dilution LC-MRM/MS assay for all eight (\pm)-*trans*-B[a]PDE-derived DNA-adducts will

make it possible to examine how these manipulations affect CYP-mediated DNA damage. This will allow the relative importance of the CYP and AKR pathways of B[a]P-mediated DNA damage to be assessed. Finally, this method will be used in combination with immunopurification methodology for the analysis of urinary adducts and with higher sensitivity nanospray ionization for analysis of B[a]PDE-derived adducts in tissue DNA.

Acknowledgements

We thank the NIH for financial support through grant P01 CA 92537. We also thank Dr. Nicolas E. Geacintov for providing the CD spectrometer facility and Dr. Michael Pollack for editorial assistance.

REFERENCES

- Baird WM, Hooven LA, Mahadevan B. *Environ. Mol. Mutagen.* 2005; **45**: 106. DOI: 10.1002/em.20095.
- Lee LL, Lee JS, Waldman SD, Casper RF, Grynepas MD. *Bone* 2002; **30**: 917. DOI: 10.1016/S8756-3282(02)00726-3.
- Rothman N, Shields PG, Poirier MC, Harrington AM, Ford DP, Strickland PT. *Mol. Carcinog.* 1995; **14**: 63.
- Grimmer G, Bohnke H. *J. Environ. Pathol. Toxicol.* 1978; **1**: 661.
- Mastrangelo G, Fadda E, Marzia V. *Environ. Health Perspect.* 1996; **104**: 1166.
- Armstrong B, Hutchinson E, Unwin J, Fletcher T. *Environ. Health Perspect.* 2004; **112**: 970. DOI: 10.1289/ehp.6895.
- Pfeifer GP, Denissenko MF, Olivier M, Tretyakova N, Hecht SS, Hainaut P. *Oncogene* 2002; **21**: 7435. DOI: 10.1038/sj.onc.1205803.
- Boffetta P, Jourenkova N, Gustavsson P. *Cancer Causes Control* 1997; **8**: 444.
- Rubin H. *Carcinogenesis* 2001; **22**: 1903.
- Xue W, Warshawsky D. *Toxicol. Appl. Pharmacol.* 2005; **206**: 73. DOI: 10.1016/j.taap.2004.11.006.
- Gelboin HV. *Physiol. Rev.* 1980; **60**: 1107.
- Smithgall TE, Harvey RG, Penning TM. *J. Biol. Chem.* 1986; **261**: 6184.
- Jiang H, Shen YM, Quinn AM, Penning TM. *Chem. Res. Toxicol.* 2005; **18**: 365. DOI: 10.1021/tx0497245.
- Cavalieri EL, Rogan EG. *Xenobiotica* 1995; **25**: 677.
- Shimada T, Gillam EM, Oda Y, Tsumura F, Sutter TR, Guengerich FP, Inoue K. *Chem. Res. Toxicol.* 1999; **12**: 623. DOI: 10.1021/tx990028s.
- Shimada T, Oda Y, Gillam EM, Guengerich FP, Inouye K. *Drug Metab. Dispos.* 2001; **29**: 1176.
- Shimada T, Hayes CL, Yamazaki H, Amin S, Hecht SS, Guengerich FP, Sutter TR. *Cancer Res.* 1996; **56**: 2979.
- Shimada T, Fujii-Kuriyama Y. *Cancer Sci.* 2004; **95**: 1. DOI: 10.1111/j.1349-7006.2004.tb03162.x.
- Reed GA, Marnett LJ. *J. Biol. Chem.* 1982; **257**: 11368.
- Ji C, Marnett LJ. *J. Biol. Chem.* 1992; **267**: 17842.
- Weston A, Bowman ED, Carr P, Rothman N, Strickland PT. *Carcinogenesis* 1993; **14**: 1053.
- Singh SV, Varma V, Zimniak P, Srivastava SK, Marynowski SW, Desai D, Amin S, Ji X. *Biochemistry* 2004; **43**: 9708. DOI: 10.1021/bi049435f.
- Burczynski ME, Harvey RG, Penning TM. *Biochemistry* 1998; **37**: 6781. DOI: 10.1021/bi972725u.
- Palackal NT, Burczynski ME, Harvey RG, Penning TM. *Biochemistry* 2001; **40**: 10901. DOI: 10.1021/bi010872t.
- Palackal NT, Lee SH, Harvey RG, Blair IA, Penning TM. *J. Biol. Chem.* 2002; **277**: 24799. DOI: 10.1074/jbc.M112424200.
- Shou M, Harvey RG, Penning TM. *Carcinogenesis* 1993; **14**: 475.
- McCoull KD, Rindgen D, Blair IA, Penning TM. *Chem. Res. Toxicol.* 1999; **12**: 237. DOI: 10.1021/tx980182z.
- Balu N, Padgett WT, Lambert GR, Swank AE, Richard AM, Nesnow S. *Chem. Res. Toxicol.* 2004; **17**: 827. DOI: 10.1021/tx034207s.
- Flowers L, Ohnishi ST, Penning TM. *Biochemistry* 1997; **36**: 8640. DOI: 10.1021/bi970367p.
- Park JH, Gopishetty S, Szewczuk LM, Troxel AB, Harvey RG, Penning TM. *Chem. Res. Toxicol.* 2005; **18**: 1026. DOI: 10.1021/tx050001a.
- Cavalieri EL, Rogan EG. *Free Radical Res. Commun.* 1990; **11**: 77.
- Cavalieri EL, Rogan EG. *Pharmacol. Ther.* 1992; **55**: 183. DOI: 10.1016/0163-7258(92)90015-R.
- Malaveille C, Kuroki T, Sims P, Grover PL, Bartsch H. *Mutat. Res.* 1977; **44**: 313.
- Wood AW, Chang RL, Levin W, Yagi H, Thakker DR, Jerina DM, Conney AH. *Biochem. Biophys. Res. Commun.* 1977; **77**: 1389.
- Buening MK, Wislocki PG, Levin W, Yagi H, Thakker DR, Akagi H, Koreeda M, Jerina DM, Conney AH. *Proc. Natl. Acad. Sci. USA* 1978; **75**: 5358.
- Kapitulnik J, Wislocki PG, Levin W, Yagi H, Jerina DM, Conney AH. *Cancer Res.* 1978; **38**: 354.
- Chang RL, Wood AW, Conney AH, Yagi H, Sayer JM, Thakker DR, Jerina DM, Levin W. *Proc. Natl. Acad. Sci. USA* 1987; **84**: 8633.
- Sram RJ, Binkova B. *Environ. Health Perspect.* 2000; **108**: 57.
- Banasiewicz M, Nelson G, Swank A, Grubor N, Ross J, Nesnow S, Kofeler H, Small GJ, Jankowiak R. *Anal. Biochem.* 2004; **334**: 390. DOI: 10.1016/j.ab.2004.08.006.
- Beland FA, Churchwell MI, Von Tungeln LS, Chen S, Fu PP, Culp SJ, Schoket B, Gyorffy E, Minarovits J, Poirier MC, Bowman ED, Weston A, Doerge DR. *Chem. Res. Toxicol.* 2005; **18**: 306. DOI: 10.1021/tx050068y.
- Chen YL, Wang CJ, Wu KY. *Rapid Commun. Mass Spectrom.* 2005; **19**: 893. DOI: 10.1002/rcm.1868.
- Matter B, Wang G, Jones R, Tretyakova N. *Chem. Res. Toxicol.* 2004; **17**: 731. DOI: 10.1021/tx0499741.
- Tretyakova N, Matter B, Jones R, Shalloo A. *Biochemistry* 2002; **41**: 9535. DOI: 10.1021/bi025540i.
- Gennaro LA, Vadhanam M, Gupta RC, Vouros P. *Rapid Commun. Mass Spectrom.* 2004; **18**: 1541. DOI: 10.1002/rcm.1516.
- Pulkrabek P, Leffler S, Weinstein IB, Grunberger D. *Biochemistry* 1977; **16**: 3127.
- Geacintov NE, Gagliano AG, Ibanez V, Harvey RG. *Carcinogenesis* 1982; **3**: 247.
- Geacintov NE, Cosman M, Mao B, Alfano A, Ibanez V, Harvey RG. *Carcinogenesis* 1991; **12**: 2099.
- Sayer JM, Chadha A, Agarwal SK, Yeh HJC, Yagi H, Jerina DM. *J. Org. Chem.* 1991; **56**: 20. DOI: 10.1021/jo00001a007.
- Szeliga J, Dipple A. *Chem. Res. Toxicol.* 1998; **11**: 1. DOI: 10.1021/tx970142f.
- Levin W, Wood AW, Chang RL, Slaga TJ, Yagi H, Jerina DM, Conney AH. *Cancer Res.* 1977; **37**: 2721.
- Roche CJ, Jeffrey AM, Mao B, Alfano A, Kim SK, Ibanez V, Geacintov NE. *Chem. Res. Toxicol.* 1991; **4**: 311. DOI: 10.1021/tx00021a009.
- Buterin T, Hess MT, Luneva N, Geacintov NE, Amin S, Kroth H, Seidel A, Naegeli H. *Cancer Res.* 2000; **60**: 1849.
- Dreij K, Seidel A, Jernstrom B. *Chem. Res. Toxicol.* 2005; **18**: 655. DOI: 10.1021/tx0497090.
- Fernandes A, Liu T, Amin S, Geacintov NE, Grollman AP, Moriyan M. *Biochemistry* 1998; **37**: 10164. DOI: 10.1021/bi980401f.
- Conney AH. *Cancer Res.* 1982; **42**: 4875.
- Jiang H, Vudathala DK, Blair IA, Penning TM. *Chem. Res. Toxicol.* 2006; **19**: 68. DOI: 10.1074/jbc.M112424200.